

Diffraction-free optical beam propagation with near-zero phase variation in extremely anisotropic metamaterials

Lei Sun, Xiaodong Yang,^{*} Wei Wang, and Jie Gao[†]

Department of Mechanical and Aerospace Engineering,

Missouri University of Science and Technology,

Rolla, Missouri 65409, USA

Abstract

Extremely anisotropic metal-dielectric multilayer metamaterials are designed to have the effective permittivity tensor of a transverse component (parallel to the interfaces of the multilayer) with zero real part and a longitudinal component (normal to the interfaces of the multilayer) with ultra-large imaginary part at the same wavelength, including the optical nonlocality analysis based on the transfer-matrix method. The diffraction-free deep-subwavelength optical beam propagation with near-zero phase variation in the designed multilayer stack due to the near-flat iso-frequency contour is demonstrated and analyzed, including the effects of the multilayer period and the material loss.

^{*} Electronic address: yangxia@mst.edu

[†] Electronic address: gaojie@mst.edu

I. INTRODUCTION

Light beam propagating beyond diffraction limit with deep-subwavelength confinement and near-zero phase variation is highly desirable in many optical integration applications. In order to realize such intriguing optical beam propagation phenomena, optical materials are required to possess an extremely anisotropic effective refractive index tensor with an ultra-high component perpendicular to the propagation direction to support the light beam of large wave vector and an ultra-low component in the propagation direction to reduce the phase variation of the light beam simultaneously. Optical metamaterials with artificial subwavelength meta-atoms and tunable effective permittivity and effective permeability have been designed to exhibit ultra-high effective refractive index so as to achieve large wave vectors [1, 2], as well as to have zero effective refractive index for obtaining the optical beam propagation with zero phase variation [3, 4]. Among all these designs, the metal-dielectric multilayer metamaterials are of great interest in demonstrating many exciting applications such as negative refraction [5], epsilon-near-zero (ENZ) materials [6–9], and epsilon-near-pole (ENP) materials [10]. Particularly, possessing an indefinite permittivity tensor, the multilayer metamaterials are of unique applications in subwavelength imaging [11, 12], enhanced photonic density of states [13], broadband light absorbers [14–16], ultra-high refractive indices for subwavelength optical waveguides [17], indefinite cavities [18, 19], broadband spontaneous emission engineering [20–22], super-Planck thermal emission [23–25], ultra-large-wavevector plasmon polaritons [26–28], and other exceptional properties [29–31].

In our previous work [32], the extremely loss-anisotropic metal-dielectric multilayer metamaterials are designed in order to realize the diffraction-free optical beam propagation mainly based on the effective medium theory (EMT) and the operation wavelength is adjusted from the dispersion relation of the multilayer stack. However, the effective permittivity tensor including the optical nonlocality is not well considered in the analysis. Therefore, in the present work, a new kind of metal-dielectric multilayer metamaterials are designed to have the extremely anisotropic effective permittivity tensor for the demonstration of both the diffraction-free optical beam propagation and the near-zero phase variation along the propagation direction, based on a theoretical analysis of the effective permittivity tensor including the optical nonlocality. The designed multilayer metamaterials will have the effective permittivity tensor with a near-zero transverse component parallel to the multilayer

and an ultra-large longitudinal component in the imaginary part normal to the multilayer at the same wavelength, which represents the ENZ-ENP wavelength. The near-zero transverse component of the effective permittivity tensor leads to the near-zero phase variation during the propagation of the electromagnetic wave. On the other hand, the longitudinal component with an ultra-large imaginary part of the effective permittivity tensor will reduce the diffraction of the electromagnetic wave [33, 34]. The filling ratio of metal in the metal-dielectric multilayer stack with respect to the ENZ-ENP wavelength is fully analyzed according to the transfer-matrix method including the optical nonlocality, while the performance of the deep-subwavelength optical beam propagation with near-zero phase variation is also explored with respect to the variation of the material loss. In the following sections, the diffraction-free optical beam propagation with near-zero phase variation is discussed in theoretical analysis based on EMT and optical nonlocality, together with numerical simulation in Sec. 2, followed by the conclusion in Sec. 3.

II. THEORY AND DISCUSSION

A. Effective medium theory and optical nonlocality

Illustrated in Fig. 1(a), the metal-dielectric multilayer stack is composite of alternating layers of silver (Ag) and titanium pentoxide (Ti_3O_5), with the thickness a_m and a_d , respectively. The permittivity of Ag follows the Drude model $\varepsilon_m = \varepsilon_\infty - \omega_p^2/(\omega^2 + i\omega\gamma)$, with the permittivity constant $\varepsilon_\infty = 5.7$, the plasma frequency $\omega_p = 1.37 \times 10^{16}$ rad/s, and the damping factor $\gamma = \Delta \cdot (8.5 \times 10^{13})$ rad/s. According to the previous experimental demonstration [35], the material loss of Ag can be reduced by the annealing process so that the damping factor γ is decreased. Here the damping factor ratio Δ is included in order to tune the material loss of Ag and is set to be $\Delta = 0.1$ in the following analysis. The permittivity of Ti_3O_5 is $\varepsilon_d = 5.83$. When the thickness of each layer is sufficiently small, i.e., $|ka| \ll 1$, where k is the wave vector in the layer and a is the thickness of the layer [36], the multilayer stack can be regarded as a homogeneous anisotropic effective medium with a permittivity tensor based on the EMT

$$\begin{aligned}\varepsilon_{xy}^{\text{EMT}} &= f_m \varepsilon_m + f_d \varepsilon_d, \\ \varepsilon_z^{\text{EMT}} &= (f_m/\varepsilon_m + f_d/\varepsilon_d)^{-1},\end{aligned}\tag{1}$$

which is related to the filling ratio of Ag and Ti_3O_5 , $f_m = a_m/(a_m+a_d)$ and $f_d = a_d/(a_m+a_d)$. According to Eq. (1), it is interesting that if the real part of the permittivity of Ag is greater than that of the imaginary part, i.e., $\text{Re}(\varepsilon_m) \gg \text{Im}(\varepsilon_m)$, the EMT-based ENZ wavelength (where $\text{Re}(\varepsilon_{xy}^{\text{EMT}}) = 0$) and the EMT-base ENP wavelength (where the maximum of $\text{Im}(\varepsilon_z^{\text{EMT}})$ is obtained) can be approximately associated with the EMT-based filling ratio of Ag as $f_m^{\text{EMT}} \approx \varepsilon_d/(\varepsilon_d - \text{Re}(\varepsilon_m))$ and $f_m^{\text{EMT}} \approx -\text{Re}(\varepsilon_m)/(\varepsilon_d - \text{Re}(\varepsilon_m))$, respectively. Therefore, the EMT-based ENZ-ENP wavelength is related to the approximate condition of $\varepsilon_d = -\text{Re}(\varepsilon_m)$, which implies that once the EMT-based ENZ wavelength overlaps with the EMT-based ENP wavelength, the EMT-based filling ratio of Ag should be $f_m^{\text{EMT}} \approx 1/2$. Further algebraic calculation indicates that the accuracy result of the EMT-based filling ratio of Ag is $f_m^{\text{EMT}} = 0.500$, with respect to the permittivity of Ag in terms of Drude model and the permittivity of Ti_3O_5 . Correspondingly, the EMT-based effective permittivity tensor reads $\varepsilon_{xy}^{\text{EMT}} = 0.000 + 0.012i$ and $\varepsilon_z^{\text{EMT}} = 7.238 + 2798.497i$, presenting an extremely anisotropic permittivity property of the multilayer stack. Regarding a TM-polarized light with non-vanishing E_x , H_y , and E_z field components propagating along the z -direction in the x - z plane, the iso-frequency contour (IFC) of the multilayer stack reads

$$k_x^2/\varepsilon_z^{\text{EMT}} + k_z^2/\varepsilon_{xy}^{\text{EMT}} = k_0^2, \quad (2)$$

while considering the extremely anisotropic permittivity property, i.e., $|\varepsilon_z^{\text{EMT}}| \gg 1 \gg |\varepsilon_{xy}^{\text{EMT}}| \approx 0$ at the EMT-based ENZ-ENP wavelength, the IFC equation in Eq. (2) can be approximately written as

$$\begin{aligned} k_z/k_0 &= \sqrt{\varepsilon_{xy}^{\text{EMT}} (1 - (k_x/k_0)^2) / \varepsilon_z^{\text{EMT}}} \\ &\approx \sqrt{\varepsilon_{xy}^{\text{EMT}}} - \sqrt{\varepsilon_{xy}^{\text{EMT}}} (k_x/k_0)^2 / (2\varepsilon_z^{\text{EMT}}). \end{aligned} \quad (3)$$

Therefore, as shown in Fig. 1(b), according to Eq. (3), the IFC of the multilayer stack at the EMT-based ENZ-ENP wavelength forms flat lines of the value $k_z/k_0 \approx (\varepsilon_{xy}^{\text{EMT}})^{1/2}$ with respect to a wide k_x/k_0 wave vector range, which leads to a diffraction-free optical beam propagation in the multilayer stack since all spatial components propagate with the same phase velocity along the z -direction. Furthermore, due to the fact that $\text{Re}(\varepsilon_{xy}^{\text{EMT}}) = 0$ and $|\varepsilon_{xy}^{\text{EMT}}| \ll 1$, the phase variation of the diffraction-free optical beam propagation in the multilayer stack is close to zero.

However, previous studies show that the metal-dielectric multilayer stack possesses strong optical nonlocality [36–39], leading to the effective permittivity tensor not only related to the

frequency but also to the wave vector, especially when the frequency approaches to the ENZ position of the structure. Such optical nonlocality can be analyzed via the transfer-matrix method, in which the multilayer stack is considered as a one-dimensional photonic crystal with the dispersion relation to the TM-polarized light as

$$\begin{aligned} \cos(k_z(a_m + a_d)) &= \cos(k_m a_m) \cos(k_d a_d) \\ &- (\varepsilon_m k_d / \varepsilon_d k_m + \varepsilon_d k_m / \varepsilon_m k_d) / 2 \sin(k_m a_m) \sin(k_d a_d), \end{aligned} \quad (4)$$

with the wave vector $k_i = \sqrt{\varepsilon_i k_0^2 - k_x^2}$ for $i = m, d$. Accordingly, the effective permittivity component in x - and y -direction including the optical nonlocality reads

$$\begin{aligned} \varepsilon_{xy}^{\text{nonloc}} &= \arccos^2[\cos(\sqrt{\varepsilon_m} k_0 a_m) \cos(\sqrt{\varepsilon_d} k_0 a_d) \\ &- (\sqrt{\varepsilon_m / \varepsilon_d} + \sqrt{\varepsilon_d / \varepsilon_m}) / 2 \sin(\sqrt{\varepsilon_m} k_0 a_m) \sin(\sqrt{\varepsilon_d} k_0 a_d)] / (k_0^2 (a_m + a_d)^2). \end{aligned} \quad (5)$$

On the other hand, the nonlocal effective permittivity component in the z -direction can be analytically obtained according to the effective permittivity definition $\varepsilon_z^{\text{nonloc}} = \langle D_z \rangle / \langle E_z \rangle$ based on the transfer-matrix method. Due to the optical nonlocality, the nonlocal ENZ wavelength and the nonlocal ENP wavelength for the multilayer stack will be different from the EMT-based ENZ-ENZ wavelength. Therefore, modification on the multilayer geometry is necessary for a certain period of $a_m + a_d$, in order to exactly overlap the nonlocal ENZ wavelength with the nonlocal ENP wavelength. Figure 1(c) shows an example about the nonlocal effective permittivity components for a multilayer stack with the period of $a_m + a_d = 20$ nm. Compared with the EMT results, the nonlocal results clearly indicate the shift of the ENZ-ENZ wavelength from the EMT calculated position of $\lambda_c^{\text{EMT}} = 466.896$ nm to the new position of $\lambda_c^{\text{nonloc}} = 468.424$ nm, while the nonlocal effective permittivity components are $\varepsilon_{xy}^{\text{nonloc}} = 0.000 + 0.012i$ and $\varepsilon_z^{\text{nonloc}} = 7.214 + 2800.879i$. Furthermore, the filling ratio of Ag related to the optical nonlocality (nonlocal filling ratio for short) also slightly changes to $f_m^{\text{nonloc}} = 0.501$, with respect to the period of the multilayer stack. In more detail, Figs. 2(a-b) individually display the variations of the filling ratio of Ag and the ENZ-ENZ wavelength with respect to different periods of the multilayer stack caused by the optical nonlocality. For comparison, the EMT results are also plotted. It is clear that as the multilayer stack period gets larger, the nonlocal filling ratio of Ag increases and the nonlocal ENZ-ENZ wavelength also shifts to a longer wavelength.

B. Diffraction-free and near-zero phase variation propagation

Based on the finite element method (FEM), the diffraction-free optical beam propagation with near-zero phase variation is demonstrated according to the numerical simulation in terms of two anti-phase TM-polarized Gaussian beams that are excited via the stimulating port boundary condition with an initial electric field distribution following the Gaussian distribution function as $\exp(-(x + c_0)^2/w_0^2)$, where c_0 determines the beam center and w_0 determines the waist size. Otherwise, the scattering boundary condition is applied to prevent the unwanted scattering from other boundaries of the simulation region. The simulation results are presented as the amplitude of the electric field, normalized by the maximum value. Figure 3 shows the calculated optical beam propagation of the Gaussian beams with ultra-narrow beam waists of $w_0 = 25$ nm in the homogeneous anisotropic effective medium at the EMT-based ENZ-ENP wavelength of $\lambda_c^{\text{EMT}} = 466.896$ nm. Besides, Fig. 4 shows the optical beam propagation results calculated in the 20 nm-period multilayer stack at the nonlocal ENZ-ENP wavelength $\lambda_c^{\text{nonloc}} = 468.424$ nm. As shown in Figs. 3(a) and 4(a), it is clear that the deep-subwavelength Gaussian beams can propagate over a long distance ($> 2\lambda_c^{\text{nonloc}}$) without any wave front distortion. At the same time, near-zero phase variation is also obtained along the propagation direction. The centre-to-centre distance of 120 nm for the two deep-subwavelength Gaussian beams remains well-defined as the beams propagating across the multilayer stack from the bottom to the top. It is noted that the confinement and propagation of the deep-subwavelength Gaussian beam inside the multilayer stack is entirely due to the unique extremely anisotropic permittivity property, and the optical beam path is well determined by the beam launching position, which is distinguished from the situation in a subwavelength optical waveguide [17], where the optical mode is confined by the waveguide boundary. Besides the straight optical beam propagation, the flow of light can be flexibly modeled through controlling the local geometry of the multilayer stack. For instance, the beam path can be manipulated by gradually varying the direction of multilayers, since the direction of the optical beam propagation is always vertical to the multilayer interface. The designed geometries for achieving 90° and 180° bending of deep-subwavelength Gaussian beams and the simulation results are shown in Figs. 3(b–c) and 4(b–c), for the effective medium and the multilayer stack, respectively. It is noted that for the effective medium the anisotropic effective permittivity tensor is transformed according

to the geometric relation between the global xyz -coordinates and the local vuw -coordinates based on the transformation optics as

$$\overset{\leftrightarrow}{\varepsilon}(x, z) = \begin{pmatrix} \varepsilon_u \cos^2 \theta + \varepsilon_w \sin^2 \theta & (\varepsilon_u - \varepsilon_w) \sin \theta \cos \theta \\ (\varepsilon_u - \varepsilon_w) \sin \theta \cos \theta & \varepsilon_u \sin^2 \theta + \varepsilon_w \cos^2 \theta \end{pmatrix}. \quad (6)$$

The results indicate that the flow of light can indeed be manipulated while maintaining the diffraction-free propagation with near-zero phase variation. For comparison, Fig. 4(d) presents the optical beam propagation at the wavelength of $\lambda = 464 \text{ nm}$, which is off the nonlocal ENZ-ENP wavelength of the 20 nm-period multilayer stack, while the corresponding nonlocal effective permittivity components read $\varepsilon_{xy}^{\text{nonloc}}|_{\lambda=464 \text{ nm}} = 0.121 + 0.012i$ and $\varepsilon_z^{\text{nonloc}}|_{\lambda=464 \text{ nm}} = -336.266 + 42.895i$. It is clear that by overlapping the ENZ wavelength and the ENP wavelength, the multilayer stack with such an extremely anisotropic effective permittivity tensor supports diffraction-free propagation with near-zero phase variation. Also, it implies that the diffraction-free propagation supported by the anisotropic effective permittivity tensor is not extremely sensitive to the value of wavelength, but for the near-zero phase variation, the ENZ wavelength must be satisfied.

In the previous analysis, the damping factor ratio of Ag is set as $\Delta = 0.1$ in order to maintain a small material loss to extend the propagation distance of the Gaussian beams. In fact, the variation of the damping factor in the Drude model will affect the optical beam propagation loss and the phase variation. Figure 5(a) represents the variation of the propagation length and the effective refractive index along the propagation direction with respect to different damping factor ratios of Ag. The effective refractive index is defined based on the nonlocal effective permittivity component as $n_z = (\varepsilon_{xy}^{\text{nonloc}})^{1/2}$ according to Eq. (5). The real part of the effective refractive index $\text{Re}(n_z)$ is proportional to the phase variation of the propagating beam, while the imaginary part $\text{Im}(n_z)$ is inversely proportional to the propagation length of the beam as $\lambda/(4\pi\text{Im}(n_z))$, where λ is the wavelength of the beam in free space. It is clear that as the damping factor ratio of Ag gets larger, the real part of the effective refractive index increases, leading to an obvious beam phase variation along the propagation direction. On the other hand, the propagation length also decreases as the material loss gets higher. Figures 5(b–d) show the propagation of the two anti-phase Gaussian beams in the 20 nm-period multilayer stack with different damping factor ratio of $\Delta = 0.1, 0.5, \text{ and } 1.0$ at the nonlocal ENZ-ENP wavelengths, illustrating the dependences of propagation length and phase variation on the damping factor ratio of Ag. It is shown

that a smaller material loss will benefit the diffraction-free and near-zero phase variation optical beam propagation in the multilayer stack.

Finally, it is worth mentioning that according to the previous experimental work of optical hyperlens [11], our above theoretical analysis of extremely anisotropic metamaterials can be realized in experiments. The ultra-narrow Gaussian beams can be achieved by inscribing nanometer scale slots or holes into a thin chrome layer coated on the top of the sample surface, while the impedance matching substrate can be applied at the bottom of the multilayer stack in order to reduce the reflection caused by the mismatched impedance.

III. CONCLUSIONS

To conclude, extremely anisotropic metal-dielectric multilayer metamaterials with identical ENZ wavelength and ENP wavelength have been designed based on the transfer-matrix method including the optical nonlocality. Such metamaterial possesses a near-flat IFC with wave vector values close to zero over a broad wave vector range. This unique property is utilized to obtain the diffraction-free deep-subwavelength optical beam propagation with near-zero phase variation, and it is demonstrated that the optical beam propagation can be manipulated flexibly by tuning the direction of the multilayer stack. The influences of multilayer period and material loss on the optical beam propagation are also studied. The current study is of great potentials in many applications such as optical imaging, optical integration, and on-chip optical communication.

ACKNOWLEDGEMENTS

This work was supported by the Intelligent Systems Center and the Energy Research and Development Center at Missouri S&T, the University of Missouri Interdisciplinary Intercampus Research Program, the Ralph E. Powe Junior Faculty Enhancement Award, and the National Science Foundation under grant CBET-1402743.

[1] Shin J, Shen J T and Fan S 2009 Three-dimensional metamaterials with an ultrahigh effective refractive index over a broad bandwidth *Phys. Rev. Lett.* **102** 093903

- [2] Choi M, Lee S H, Kim Y, Kang S B, Shin J, Kwak M H, Kang K Y, Lee Y H, Park N and Min B 2011 A terahertz metamaterial with unnaturally high refractive index *Nature* **470** 369–73
- [3] Huang X, Lai Y, Hang Z H, Zheng H and Chan C T 2011 Dirac cones induced by accidental degeneracy in photonic crystals and zero-refractive-index materials *Nat. Materials* **10** 582–6
- [4] Vesseur E J R, Coenen T, Caglayan H, Engheta N and Polman A 2013 Experimental verification of $n = 0$ structures for visible light *Phys. Rev. Lett.* **110** 013902
- [5] Valentine J, Zhang S, Zentgraf T, Ulin-Avila E, Genov D A, Bartal G and Zhang X 2008 Three-dimensional optical metamaterial with a negative refractive index *Nature* **455** 376–9
- [6] Maas R, Parsons J, Engheta N and Polman A 2013 Experimental realization of an epsilon-near-zero metamaterial at visible wavelengths *Nat. Photonics* **7** 907–12
- [7] Gao J, Sun L, Deng H, Mathai C J, Gangopadhyay S and Yang X 2013 Experimental realization of epsilon-near-zero metamaterial slabs with metal-dielectric multilayers *Appl. Phys. Lett.* **103** 051111
- [8] Sun L, Gao J and Yang X 2013 Giant optical nonlocality near the Dirac point in metal-dielectric multilayer metamaterials *Opt. Express* **21** 21542–55
- [9] Sun L, Cheng F, Mathai C J, Gangopadhyay S, Gao J and Yang X 2014 Experimental characterization of optical nonlocality in metal-dielectric multilayer metamaterials *Opt. Express* **22** 22974–80
- [10] Molesky S, Dewalt C J and Jacob Z 2013 High temperature epsilon-near-zero and epsilon-near-pole metamaterial emitters for thermophotovoltaics *Opt. Express* **21** A96–A110
- [11] Liu Z, Lee H, Xiong Y, Sun C and Zhang X 2007 Far-field optical hyperlens magnifying sub-diffraction-limited objects *Science* **315** 1686
- [12] Zhang X and Liu Z 2008 Superlenses to overcome the diffraction limit *Nat. Materials* **7** 435–41
- [13] Krishnamoorthy H N S, Jacob Z, Narimanov E, Kretzschmar I and Menon V M 2012 Topological Transitions in Metamaterials *Science* **336** 205–9
- [14] Cui Y, Fung K H, Xu J, Ma H, Jin Y, He S and Fang N X 2012 Ultrabroadband light absorption by a sawtooth anisotropic metamaterial slab *Nano Lett.* **12** 1443–7
- [15] Guclu C, Campione S and Capolino F 2012 Hyperbolic metamaterial as super absorber for scattered fields generated at its surface *Phys. Rev. B* **86** 205130
- [16] Narimanov E E, Li H, Barnakov Yu A, Tumkur T U and Noginov M A 2013 Reduced reflection from roughened hyperbolic metamaterial *Opt. Express* **21** 14956–61

- [17] He Y, He S, Gao J and Yang X 2012 Nanoscale metamaterial optical waveguides with ultrahigh refractive indices *J. Opt. Soc. Am. B* **29** 2559–66
- [18] Yao J, Yang X, Yin X, Bartal G and Zhang X 2011 Three-dimensional nanometer-scale optical cavities of indefinite medium *Proc. Natl. Acad. Sci. U. S. A.* **108** 11327–31
- [19] Yang X, Yao J, Rho J, Yin X and Zhang X 2012 Experimental realization of three-dimensional indefinite cavities at the nanoscale with anomalous scaling laws *Nat. Photonics* **6** 450–4
- [20] Noginov M A, Li H, Barnakov Yu A, Dryden D, Nataraj G, Zhu G, Bonner C E, Mayy M, Jacob Z and Narimanov E E 2010 Controlling spontaneous emission with metamaterials *Opt. Lett.* **35** 1863–5
- [21] Kidwai O, Zhukovsky S V and Sipe J E 2011 Dipole radiation near hyperbolic metamaterials: applicability of effective-medium approximation *Opt. Lett.* **36** 3530–2
- [22] Jacob Z, Smolyaninov I I and Narimanov E E 2012 Broadband Purcell effect: radiative decay engineering with metamaterials *Appl. Phys. Lett.* **100** 181105
- [23] Biehs S -A, Tschikin M and Ben-Abdallah P 2012 Hyperbolic metamaterials as an analog of a blackbody in the near field *Phys. Rev. Lett.* **109** 104301
- [24] Guo Y, Cortes C L, Molesky S and Jacob Z 2012 Broadband super-Planckian thermal emission from hyperbolic metamaterials *Appl. Phys. Lett.* **101** 131106
- [25] Guo Y and Jacob Z 2013 Thermal hyperbolic metamaterials *Opt. Express* **21** 15014–9
- [26] Othman M A K, Guclu C and Capolino F 2013 Graphene-dielectric composite metamaterials: evolution from elliptic to hyperbolic wavevector dispersion and the transverse epsilon-near-zero condition *J. Nanophoton.* **7** 073089
- [27] Zhukovsky S V, Kidwai O and Sipe J E 2013 Physical nature of volume plasmon polaritons in hyperbolic metamaterials *Opt. Express* **21** 14982–7
- [28] Zhukovsky S V, Andryieuski A, Sipe J E and Lavrinenko A V 2014 From surface to volume plasmons in hyperbolic metamaterials: general existence conditions for bulk high- k waves in metal-dielectric and graphene-dielectric multilayers *Phys. Rev. B* **90** 155429
- [29] Cortes C L, Newman W, Molesky S and Jacob Z 2012 Quantum nanophotonics using hyperbolic metamaterials *J. Opt.* **14** 063001
- [30] Poddubny A, Iorsh I, Belov P and Kivshar Y 2013 Hyperbolic metamaterials *Nat. Photonics* **7** 948–57

- [31] Orlov A A, Zhukovsky S V, Iorsh I V and Belov P A 2014 Controlling light with plasmonic multilayers *Photonics Nanostruct.* **12** 213–30
- [32] He Y, Sun L, He S and Yang X 2013 Deep subwavelength beam propagation in extremely loss-anisotropic metamaterials *J. Opt.* **15** 055105
- [33] Feng S 2012 Loss-induced omnidirectional bending to the normal in ϵ -near-zero metamaterials *Phys. Rev. Lett.* **108** 193904
- [34] Sun L, Feng S and Yang X 2012 Loss enhanced transmission and collimation in anisotropic epsilon-near-zero metamaterials *Appl. Phys. Lett.* **101** 241101
- [35] Chen W, Thoreson M D, Ishii S, Kildishev A V and Shalaev V M 2010 Ultra-thin ultra-smooth and low-loss silver films on a germanium wetting layer *Opt. Express* **18** 5124–34
- [36] Elser J, Podolskiy V A, Salakhutdinov I and Avrutsky I 2007 Nonlocal effects in effective-medium response of nanolayered metamaterials *Appl. Phys. Lett.* **90** 191109
- [37] Orlov A A, Voroshilov P M, Belov P A and Kivshar Y S 2011 Engineered optical nonlocality in nanostructured metamaterials *Phys. Rev. B* **84** 045424
- [38] Chebykin A V, Orlov A A, Vozianova A V, Maslovski S I, Kivshar Yu S and Belov P A 2011 Nonlocal effective medium model for multilayered metal-dielectric metamaterials *Phys. Rev. B* **84** 115438
- [39] Chebykin A V, Orlov A A, Simovski C R, Kivshar Yu S and Belov P A 2012 Nonlocal effective parameters of multilayered metal-dielectric metamaterials *Phys. Rev. B* **86** 115420

FIGURE CAPTIONS

FIG. 1. (Colour online) (a) Schematic of Ag-Ti₃O₅ multilayer stack. (b) The IFC of the Ag-Ti₃O₅ multilayer stack at the EMT-based ENZ-ENP wavelength, where the wave vector k_z/k_0 possesses near-zero flat real part (red lines) and imaginary part (black lines), compared with the IFC of air (green circle). (c) The EMT-based (dashed curves) and the nonlocal (solid curves) effective permittivity components, with the marked EMT-based (dashed vertical line) and the nonlocal (solid vertical line) ENZ-ENP wavelength.

FIG. 2. (Colour online) The variation of (a) the filling ratio of Ag and (b) the ENZ-ENP wavelength with respect to different periods of the Ag-Ti₃O₅ multilayer stack with optical nonlocality, compared with the EMT-based results representing the zero-period case.

FIG. 3. (Colour online) The diffraction-free optical beam propagation with near-zero phase variation of two anti-phase deep-subwavelength TM-polarized Gaussian beams in the effective medium for the case of (a) straight propagation, (b) 90° beam bending, and (c) 180° beam bending at the EMT-based ENZ-ENP wavelength.

FIG. 4. (Colour online) The diffraction-free optical beam propagation with near-zero phase variation of two Gaussian beams in the Ag-Ti₃O₅ multilayer stack for the case of (a) straight propagation, (b) 90° beam bending, and (c) 180° beam bending at the nonlocal-based ENZ-ENP wavelength. (d) The optical beam propagation of two Gaussian beams off the nonlocal-based ENZ-ENP wavelength.

FIG. 5. (Colour online) (a) The variation of the propagation length (blue curve) and the real part of the effective refractive index (red curve) with respect to different damping factor ratios of Ag. (b–d) The diffraction-free optical beam propagation with near-zero phase variation of two Gaussian beams in the Ag-Ti₃O₅ multilayer stack with respect to the damping factor ratio of (b) $\Delta = 0.1$, (c) $\Delta = 0.5$, and (d) $\Delta = 1.0$ at the nonlocal-based ENZ-ENP wavelengths.

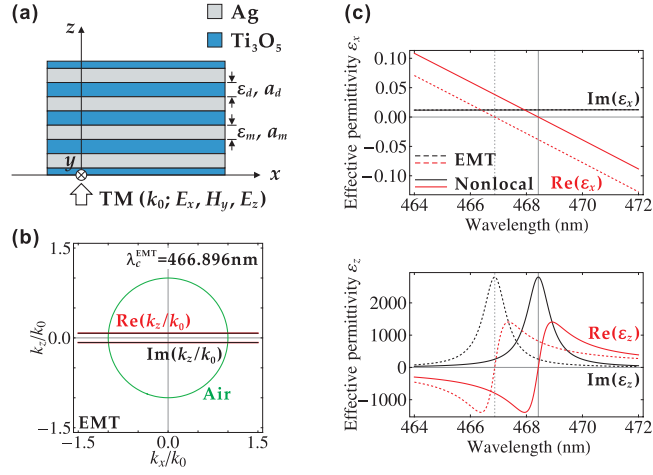


FIG. 1. Lei Sun, Xiaodong Yang, Wei Wang, and Jie Gao

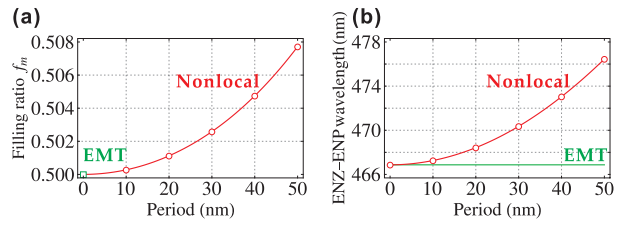


FIG. 2. Lei Sun, Xiaodong Yang, Wei Wang, and Jie Gao

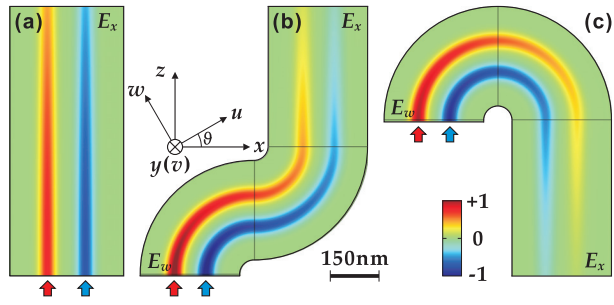


FIG. 3. Lei Sun, Xiaodong Yang, Wei Wang, and Jie Gao

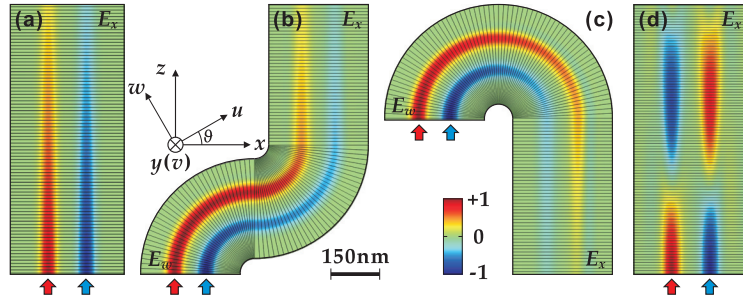


FIG. 4. Lei Sun, Xiaodong Yang, Wei Wang, and Jie Gao

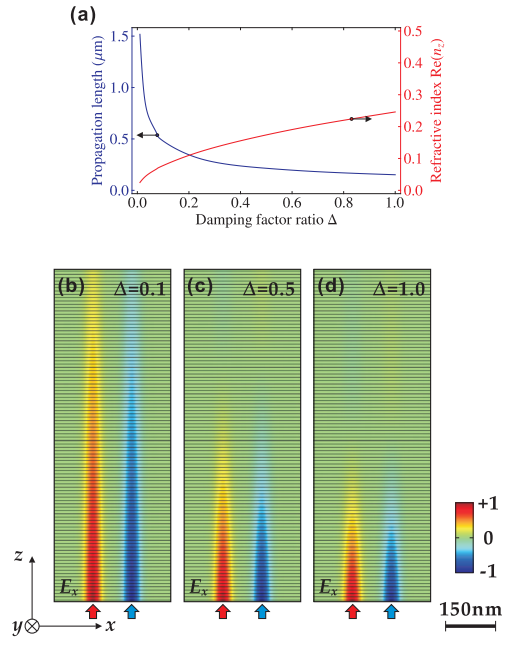


FIG. 5. Lei Sun, Xiaodong Yang, Wei Wang, and Jie Gao